Available online at www.sciencedirect.com
ScienceDirect
Acta Materialia 54 (2006) 4489–4502
Acta MATERIALIA
www.actamat-journals.com

Changes in the five-parameter grain boundary character distribution in α-brass brought about by iterative thermomechanical processing

Gregory S. Rohrer [b,*], Valerie Randle [a], Chang-Soo Kim [b,1], Yan Hu [a]

[a] Materials Research Centre, School of Engineering, University of Wales Swansea, Swansea SA2 8PP, UK
[b] Department of Materials Science and Engineering, Carnegie Mellon University, 5000 Forbes Avenue, Pittsburgh, PA 15213-3890, USA

Received 7 March 2006; received in revised form 18 May 2006; accepted 18 May 2006
Available online 14 August 2006

Abstract

This paper analyzes the changes in the five-parameter grain boundary character distribution in α-brass brought about by iterative thermomechanical processing (ITMP). In both reference and ITMP specimens, there was a tendency for boundaries to terminate on {1 1 1} planes. The high incidence of coherent twins and other boundaries terminated on {1 1 1} planes led to a high concentration of asymmetric tilt boundaries with ⟨1 1 0⟩ misorientations. After ITMP there was a larger population of coherent twins, an increase in the number fraction of Σ9 and Σ27 boundaries, an increase in the fraction of boundaries terminated on {1 1 1} planes (even when Σ3 boundaries are excluded), a decrease in the number of triple junctions with three random boundaries, and an increase in the number of triple junctions with three twin-related boundaries. The results add strength to the suggestion that 'special' boundaries are those that terminate on low-index planes.

Keywords: Electron backscattering diffraction (EBSD); Gain boundaries; Microstructure; Grain boundary engineering

1. Introduction

Iterative thermomechanical processing (ITMP) is the most well known method of manipulating the grain boundary character distribution (GBCD) of face-centred cubic (fcc) metals and alloys. ITMP frequently results in improved bulk properties, and in these cases it is referred to as 'grain boundary engineering' (GBE) [1]. For example, GBE is known to mitigate intergranular stress corrosion cracking in nickel-based alloys [2] and to influence mechanical properties such as ductility [3]. The most prominent change in the GBCD of materials produced by ITMP is an increase in the density of annealing twins and twin-related grain boundaries. It is therefore reasonable to assume that twinning is instrumental in the improvement of bulk properties. The twins, however, do not constitute part of the grain boundary network; rather they modify the crystallography of the network where they join it. How this situation can produce dramatic improvements in properties is not yet completely understood.

A decade or so ago, 'special' boundaries in GBE materials were associated with low-Σ coincident site lattice (CSL) boundaries, where Σ is the reciprocal density of coinciding sites. This categorization is based solely on the three independent parameters that specify the lattice misorientation. Grain boundary properties, on the other hand, depend on both the lattice misorientation and the orientation of the grain boundary plane. Because two additional independent parameters are required to specify the boundary plane orientation, the three-parameter CSL approach is not capable of unambiguously distinguishing between special and non-special boundaries [4]. A common example is that the energy of the 'coherent twin', which is a Σ3

* Corresponding author. Tel.: +1 412 268 2696; fax: +1 412 268 3113.
E-mail address: gr20@andrew.cmu.edu (G.S. Rohrer).
[1] Current address: Division of Chemistry and Materials Science, US Food and Drug Administration, Rockville, MD 20852, USA.

1359-6454/$30.00
doi:10.1016/j.actamat.2006.05.035

boundary with a {1 1 1} boundary plane, is much lower than that of the 'incoherent twin', which is a Σ3 boundary on a {1 1 2} boundary plane.

During the same time period as the initial GBE work, atomistic modelling and high-resolution electron microscopy (HREM) provided complementary insight into the role of the boundary plane in determining the special characteristics of a grain boundary. For example, HREM observations of ⟨1 1 0⟩ tilt boundaries in gold bicrystals showed that asymmetric boundary facets with one low-index plane were dominant between regions of symmetric boundary facets [5]. Atomistic calculations of grain boundary structure-energy correlations augmented the HREM findings. It was shown that asymmetric tilt grain boundary combinations with one low-index plane, e.g., 111/115, 100/221, 110/114 can have low energy, often lower than a symmetrical tilt grain boundary combination. More generally, a linear correlation between the energy of a grain boundary and its free volume was found [6].

There is growing evidence that grain boundary properties depend in a sensitive way on the grain boundary plane orientation. For example, studies of ⟨1 1 0⟩ symmetric tilt boundaries in Al, NiO, and MgO show that the energies of low Σ CSL boundaries depend on the orientation of the grain boundary plane [7–9]. In this situation, rotations of 70.5° and 109.4° about [1 1 0] are both Σ3 misorientations; however, a boundary made up of symmetric {1 1 1} boundary planes at 70.5° has an energy that is as much as three times lower than the boundary at 109.4°. Studies of the inclination dependence of the energy of Σ3 grain boundaries in Cu have also shown that the energy increases with the angle of inclination away from the coherent twin orientation [10,11]. A comprehensive study of grain boundary energies in MgO over all five crystallographic parameters has illustrated that the strong dependence of grain boundary energy on grain boundary orientation is a general phenomenon that occurs at all lattice misorientations [12]. The effect of grain boundary orientation on energy has also been illustrated for a single high-angle grain boundary in NiAl [13]. So, if low energy is associated with 'specialness', then the grain boundary orientation determines how special it is.

Grain boundary orientation has also been observed to be important for boundaries that are special because of their corrosion resistance, degree of segregation, or grain boundary wetting. For example, it was found that the corrosion resistance of grain boundaries in pure copper was correlated to the interplanar spacing at the boundary, but not the Σ-value [14]. Similarly, in an Fe–6% Si alloy, 37° [1 0 0] tilt grain boundaries terminated by low-index planes showed greater resistance to corrosion than those terminated by higher index planes [15]. In an Fe–3% Si alloy, twist boundaries exhibited a higher degree of segregation than did tilt boundaries [16]. Also, based on the amount of segregation to grain boundaries in Fe–Si alloy bicrystals with [1 0 0] tilt misorientations, symmetric tilt boundaries and asymmetric boundaries formed with a (1 1 0) plane were labelled as special [17]. Finally, studies of grain boundary wetting by liquid copper in an iron–copper alloy indicated that the propensity for wetting increased with the grain boundary free volume and the atomic roughness of the surfaces comprising the boundary. Furthermore, a model incorporating grain boundary plane roughness as a parameter predicted with 80% accuracy whether or not a grain boundary would be wet [18].

Measurements of the relative areas of different types of boundaries in very large sample populations as a function of all five grain boundary parameters have illustrated a clear tendency for grains to terminate on low-index planes in a variety of ceramic and metal polycrystals [19,20]. For example, in MgO, {1 0 0} grain boundary planes have been shown to occur most frequently in the population and to have the lowest relative energy [12,21]. Furthermore, there is an inverse relationship between the frequency with which boundaries occur in the population and their energy [22–24]. The relatively low energy of boundaries comprised of low-index planes arises because the energy of each grain boundary is the sum of the energies of the planes, which make up the boundary interface, minus a binding energy that comes from bringing the two surfaces together. As long as the binding energy is relatively constant, grain boundaries with low index surfaces have relatively low energies. These observations have led to the suggestion that a 'special' grain boundary is defined as one that is terminated by at least one low-index plane [20].

The observations described above have contributed to a growing body of evidence that special behaviour at grain boundaries is related to low-index planes rather than particular misorientations. We have recently reported preliminary results of measurements of the GBCD in α-brass after five strain recrystallization cycles [25]. The purpose of this paper is to compare the distribution of grain boundary planes in samples of α-brass after one and five strain-recrystallization cycles. The mechanical properties of these samples have already been reported and it was found that ITMP significantly increased the ductility of the material [26]. Considering the fact that dislocation transmission across boundaries depends on both the misorientation and the grain boundary plane orientation, the GBCD is expected to affect the ductility even when other microstructural features are unchanged [27]. By quantifying the changes in the GBCD, it is possible to identify features that might contribute to the increased ductility.

2. Methods

The α-brass specimens used in this study contained 70 wt.% Cu and 30 wt.% Zn. The ITMP was performed on flat tensile specimens with a 40 mm gauge length and a $6 \times 1\ mm^2$ cross-sectional area. For each iteration, the samples were strained in tension by 25%, annealed in air at 665 °C for 300 s, and then air cooled. The mechanical properties of these same specimens were studied previously and it was found that five iterative cycles doubled the

material's ductility [26]. Many high-resolution electron backscatter diffraction (EBSD) orientation maps of both the specimen that had received one processing iteration (referred to as 'reference') and the specimen that had received five processing iterations (referred to as 'ITMP') were obtained using HKL Channel 5 software interfaced to a Philips XL30 scanning electron microscope operated at an accelerating voltage of 20 kV. Maps were obtained by beam scanning followed by stitching together contiguous regions. A step size of 2 μm was used for mapping. The Brandon criterion was used to categorize a CSL.

A stereological method has been devised to extract the relative populations of grain boundaries as a function of all five grain boundary parameters from orientation maps in a single planar section [28]. The orientation data were used to determine the GBCD, $\lambda(\Delta g, \mathbf{n})$, which is defined as the relative areas of distinguishable grain boundaries characterized by their lattice misorientation (Δg) and boundary plane orientation ($\mathbf{n}$) [20]. The GBCD is measured in multiples of a random distribution (MRD). Each grain boundary connecting two triple points can be broken up into to several line segments, referred to as grain boundary traces. The direction of the trace and the lattice misorientation across each trace specify four of the five parameters necessary to determine the distribution; the only unknown parameter is the inclination of the boundary plane with respect to the surface. If a sufficient number of grain boundary traces from randomly orientated, symmetrically indistinguishable bicrystals are observed, then stereology can be used to specify the probability that certain grain boundary planes appear in the microstructure [28]. In this case, our data set was made up of 92,000 and 77,000 grain boundary traces from the reference and ITMP samples, respectively. These traces were extracted from the orientation maps using a procedure described by Wright and Larsen [29].

The GBCD, $\lambda(\Delta g, \mathbf{n})$, is parameterized and discretized as described in our previous work, and therefore has a resolution of approximately 10° [20]. While earlier work has indicated that this reproduces the principal features of continuous distributions, it should also be noted that any peaks in the distribution of grain boundary planes are averaged with all boundaries in a 10° window [12,21,28]. Thus, if there are cusps in the distribution, the true population will be diluted by the coarse discretization. The effect is that extreme values move closer to the average. Thus, while the discretization may cause us to underestimate the actual values at the extreme positions in the distribution, it does not alter the qualitative characteristics of the observations.

3. Results

Orientation maps from the reference and ITMP brass are shown in Fig. 1a and b, respectively. The grain size has approximately doubled after ITMP. If twins are included as boundaries which define grains on the basis of crystallography, the average crystal size in the reference and ITMP specimens is 17 and 40 μm, respectively. Table 1 shows proportions of Σ3, Σ9, and Σ27 boundaries according to both length fraction and number fraction [30]. The Σ 27 category was split almost equally between Σ27a and Σ27b. The length fraction of Σ3 boundaries has increased from 45% to 58% after ITMP processing. The number fraction is approximately two-thirds of the length fraction, because annealing twins (which make up the majority of Σ3 boundaries) tend to be long and frequently occur multiply in the same grain. In the case of both Σ9 and Σ27, the length fraction was 3% and 1%, respectively, and increased slightly during ITMP. However, in contrast to the case of Σ3 boundaries, the number fraction was approximately 1.5 times the length fraction for the reference specimen and double the length fraction for the ITMP specimen. The fraction of low-angle boundaries in both specimens was less than 2%. Grain boundaries with CSL misorientations other than Σ3, Σ 9, and Σ27 are not present at levels above those expected for a random distribution.

The distributions of boundary planes (for grain boundaries of all possible misorientations) for the reference and ITMP specimens are shown in Fig. 2a and b, respectively. The area distributions of grain boundary planes as a function of boundary normal are shown on a stereographic projection in units of MRD. In both cases, there are pronounced peaks at ⟨1 1 1⟩, with a greater area fraction for the ITMP specimen (MRD = 7.81) compared to the reference specimen (MRD = 5.21). This result is not surprising given that 45% and 58% of the interface length in the reference and ITMP specimens, respectively, is Σ3 and the morphology of these boundaries in the maps (Fig. 1) indicates that most of them are coherent twins on {1 1 1}. It is more informative therefore to view the grain boundary plane population distributions with boundaries that are close to coherent twins excluded from the distributions. Boundaries are selectively removed from the distribution if they meet the Brandon criterion for a Σ3 and if the grain boundary trace on the planar section is within 10° of the orientation expected for a coherent twin. After removing coherent twins, approximately 66,000 line segments (reference specimen) and 45,000 line segments (ITMP specimen) remained, which is still ample to produce reliable grain boundary plane statistics [28].

The distributions of planes after excluding twins are shown in Fig. 2c and d. Although the relative area fractions are reduced, there is still a peak at ⟨1 1 1⟩, with MRD values of 1.27 and 1.40 for reference and ITMP specimens, respectively. This means that {1 1 1} planes have the largest relative areas, and that this proportion has slightly increased after ITMP. Conversely, {1 0 0} boundary planes are observed with a frequency that is less than expected in a random distribution.

Sections through the five-parameter grain boundary space reveal subtle details of the distributions. In particular, it is useful to partition the space according to low-index misorientation axes, because these have geometrical significance in that tilt or twist boundaries on low-index axes

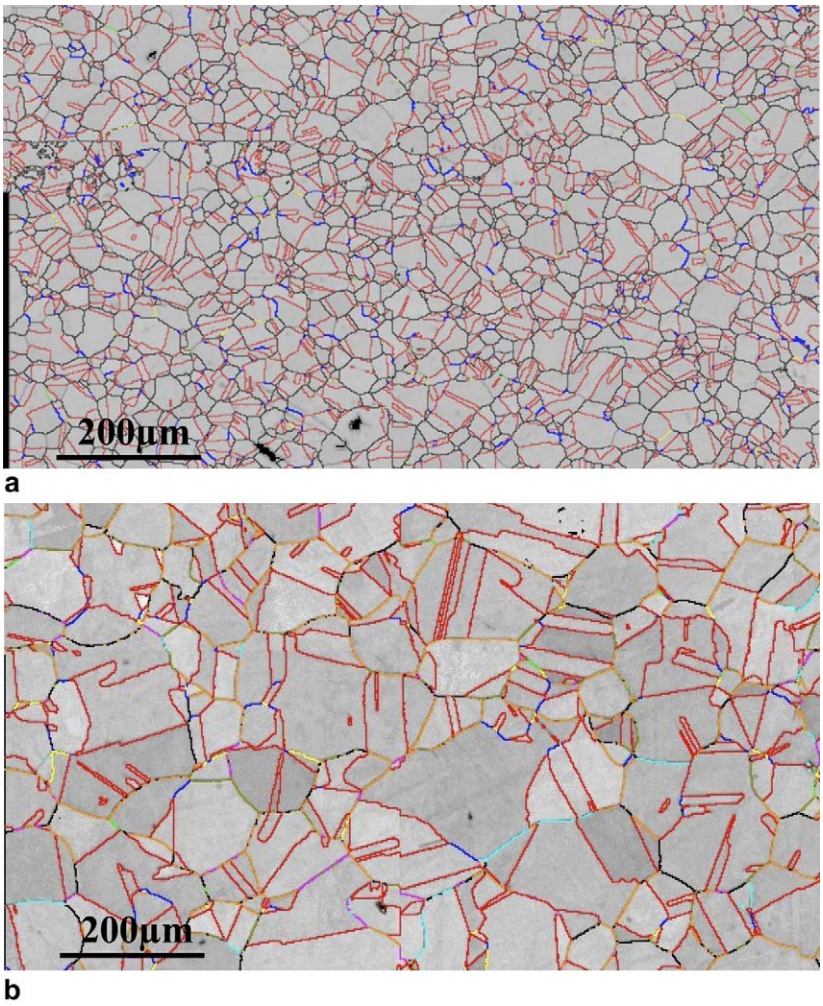

Fig. 1. Orientation maps from brass for (a) the reference sample and (b) the ITMP sample. Σ3, Σ9, and Σ27 boundaries are coloured red, blue, and yellow, respectively; other high-angle boundaries are black and low-angle boundaries are grey.

have been shown to be associated with 'special' properties, as described in Section 1. Grain boundary plane distributions for boundary misorientations about the [1 0 0], [1 1 0], and [1 1 1] axes are shown in Figs. 3–5, respectively, in misorientation angle steps of 10°. The range of angles examined covers the fundamental zone of distinguishable misorientations. As in Fig. 2c and d, coherent twins are excluded from the distributions.

In both sample populations, there are relatively few boundaries with misorientations about the [1 0 0] axis. A visual comparison of these data indicates that the repetitive strain-recrystallization cycles had no significant effect on the distribution of grain boundaries with misorientations about [1 0 0]. In these plots, pure twist boundaries occur at the [1 0 0] and $[\bar{1}\,0\,0]$ positions and pure tilt boundaries occur along the great circle (vertical line) connecting the [0 1 0] and $[0\,\bar{1}\,0]$ directions. The peaks in these distributions do not occur at either of these special positions. The ⟨1 1 1⟩ type orientations are the one low-index plane that is consistently observed more frequently than random. This corresponds to a mixed tilt-twist boundary configuration and illustrates the tendency of these boundaries to seek a low-index, close-packed plane. The ITMP leads to a small increase in the areas of the low-angle boundaries, but this is not considered significant.

Table 1
Proportions of Σ3, Σ9, and Σ27 boundaries in reference and ITMP specimens

	Reference		ITMP	
	Length fraction (%)	Number fraction (%)	Length fraction (%)	Number fraction (%)
Σ3	45.1	31.3	57.7	38.2
Σ9	3.4	5.3	3.8	6.7
Σ27	1.1	1.5	1.9	3.9

The interface plane distributions for grain boundaries with [1 1 0] misorientations are shown in Fig. 4. For each misorientation angle, there is a significant peak (between 4 and 19 MRD) in the distribution. The [1 1 0] misorientation axis is in the plane of the projection and tilt boundaries are found in the [1 1 0] zone, i.e., along the great circle (diagonal line) connecting the $[\bar{1}\,1\,0]$ and $[1\,\bar{1}\,0]$ directions.

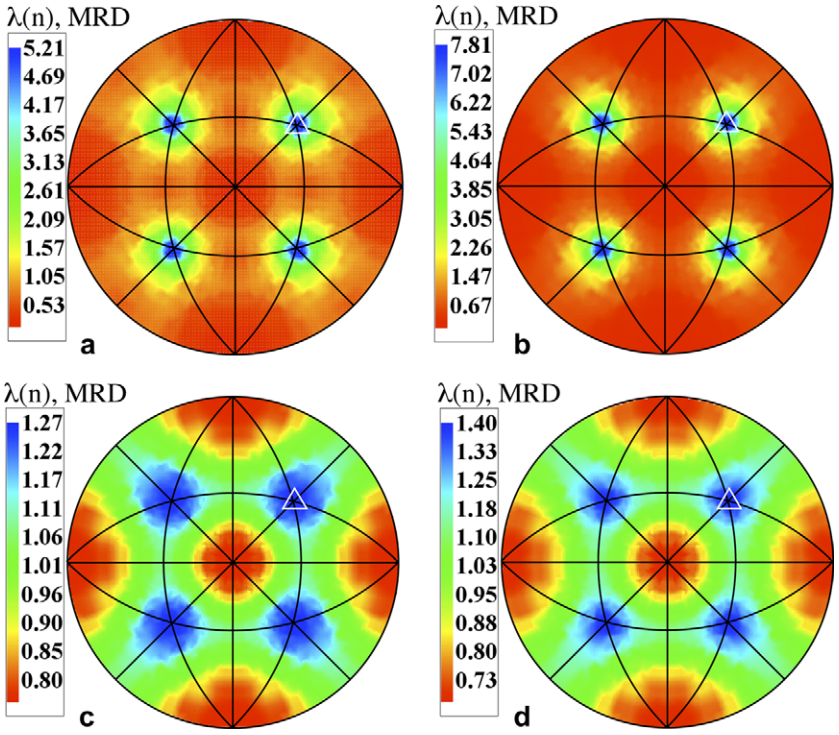

Fig. 2. Distribution of grain boundary planes, $\lambda(\mathbf{n})$, in ITMP brass specimens. (a) The distribution for all boundaries in the reference sample. (b) The distribution for all boundaries in the ITMP sample. (c) The distribution for all boundaries in the reference sample, but with coherent twins removed. (d) The distribution for all boundaries in the ITMP sample, but with coherent twins removed. The data are plotted in stereographic projection along [0 0 1] and the triangle indicates the position of the [1 1 1] direction.

It is striking that, for all misorientation angles, it is tilt-type boundaries that dominate the population. The population is greatest for misorientations of 30° and 40° about the [1 1 0] axis because these configurations are close to the lattice misorientations of the Σ27a and Σ9 CSL boundaries, respectively. For misorientations less than 60°, there are multiple maxima on each of the [1 1 0] zones, indicating that the tilt boundaries are asymmetric. The shapes of the distributions are similar before and after the ITMP. However, there are some differences. For the distribution of grain boundary planes at 30° around [1 1 0], the maxima increased significantly after ITMP whereas at 40° the maxima stayed the same and there are more mixed boundaries with orientations away from the [1 1 0] zone.

The distributions of grain boundary planes for boundaries with misorientations about the [1 1 1] axis are illustrated in Fig. 5. For all of the high-angle boundaries there is a single pronounced peak at the [1 1 1] orientation, indicating a preference for twist boundaries in which both crystals adjacent to the boundary are terminated on (1 1 1) planes. The peaks of the distribution for boundaries with misorientations about [1 1 1] are less than for those along [1 1 0]. The peaks of the distributions are slightly higher after the ITMP. In the distribution of grain boundary planes for the 60° rotation about [1 1 1], there is no clear maximum at the position 82° away from the coherent twin where the so-called 9R facet has been observed in Al bicrystals [31].

The grain boundary plane distributions for Σ9, Σ27a, and Σ27b CSL misorientations are shown in Fig. 6. To emphasize how the distributions are changed by the grain boundary engineering process, the differences between the reference and ITMP distributions are also shown. The changes in the distribution of planes for boundaries with the Σ9 misorientation are particularly interesting. Although the fraction of these boundaries increases (see Table 1), the maximum in the distribution does not increase. This means that the new Σ9 boundaries in the ITMP specimen have orientations away from the maximum and the axis of asymmetric tilt boundaries. This is clearly illustrated by the difference plot in Fig. 6c, which shows maxima near the {1 1 1} orientations. The peak on the zone of tilt boundaries is centred at the $[\bar{2}\,2\,1]$ orientation, which is a symmetric tilt. The other peaks in Fig. 6c correspond to boundaries with mixed character.

The grain boundary plane distributions for the Σ27a CSL (32°/1 1 0) are shown in Fig. 6d and e for the reference and ITMP specimens, respectively. In contrast to the Σ9 case, the ITMP increases the relative areas of asymmetric tilt boundaries. The distribution of grain boundary planes for the Σ27a CSL peaks at a higher value than the for the distribution for the Σ9 CSL, even though the length fractions listed in Table 1 show that there are more Σ9 type boundaries. This apparent contradiction arises because the discretization used for the analysis of the five-parameter data effectively fixes the acceptance criteria for each

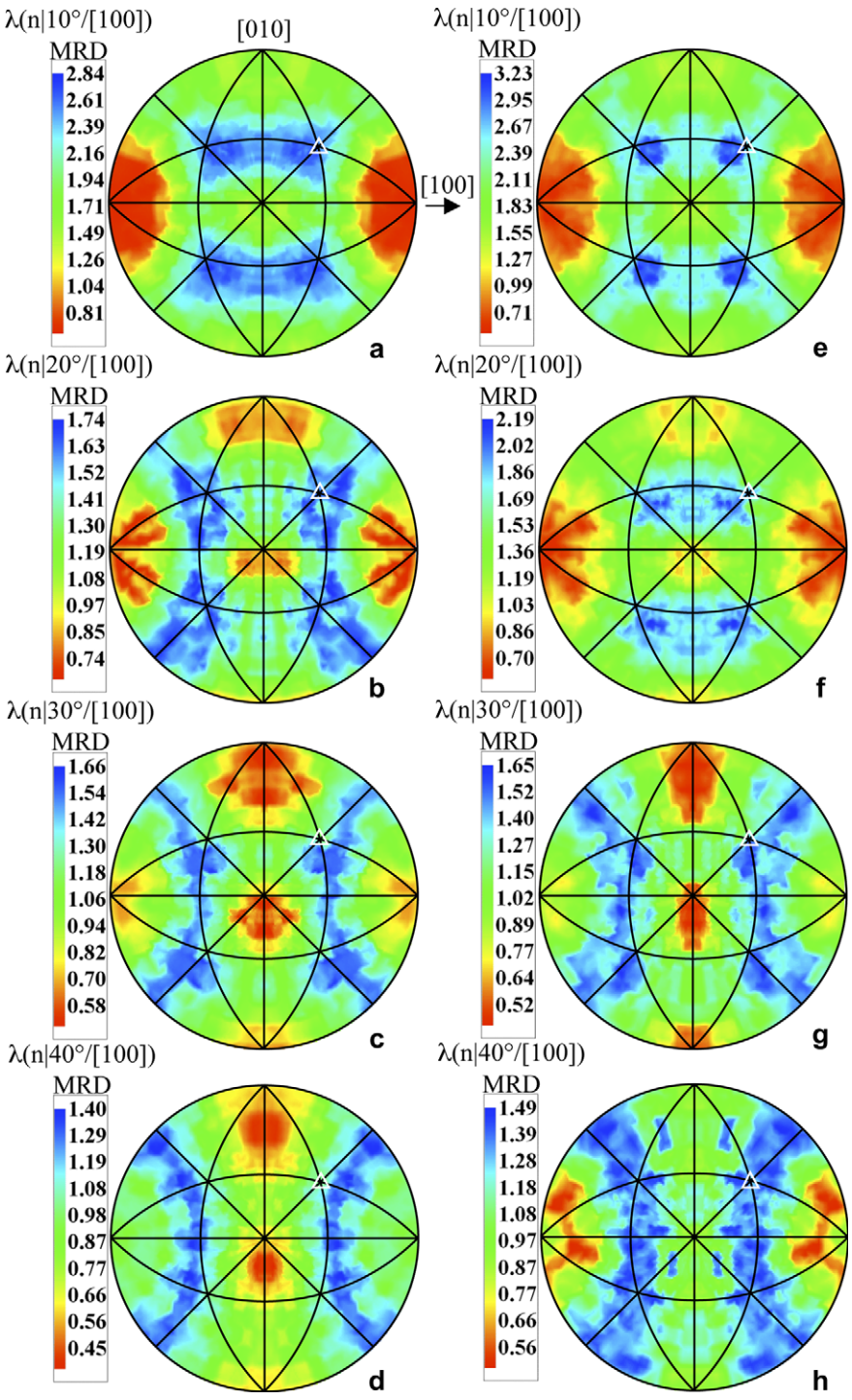

Fig. 3. Distribution of grain boundary planes for [1 0 0] misorientations, with Σ3 misorientations excluded. The misorientation angle increases in 10° increments. The data are plotted in stereographic projection along [0 0 1]. The arrow in (a) shows the direction of the [1 0 0] misorientation axis and the white triangle indicates the position of the [1 1 1] direction. Figures in the left-hand column (a–d) represent the reference sample and figures in the right-hand column (e–h) represent the ITMP sample.

CSL at a constant value of about 10°, while the length fraction calculations use the variable Brandon criterion which leads to an acceptance criterion for the Σ27a CSL that is narrower than for the Σ9 CSL.

The distribution of planes for Σ27b boundaries is interesting because it appears to lie close to the [1 1 0] zone, even though the disorientation is 35°/[2 1 0] and the [1 1 0] zone is not the zone of tilt boundaries. Furthermore, the boundaries added by the ITMP also lie on this zone. This is yet another indication that the matching of crystal planes at the grain boundary is more important than achieving a high-symmetry configuration. It should also be noted that

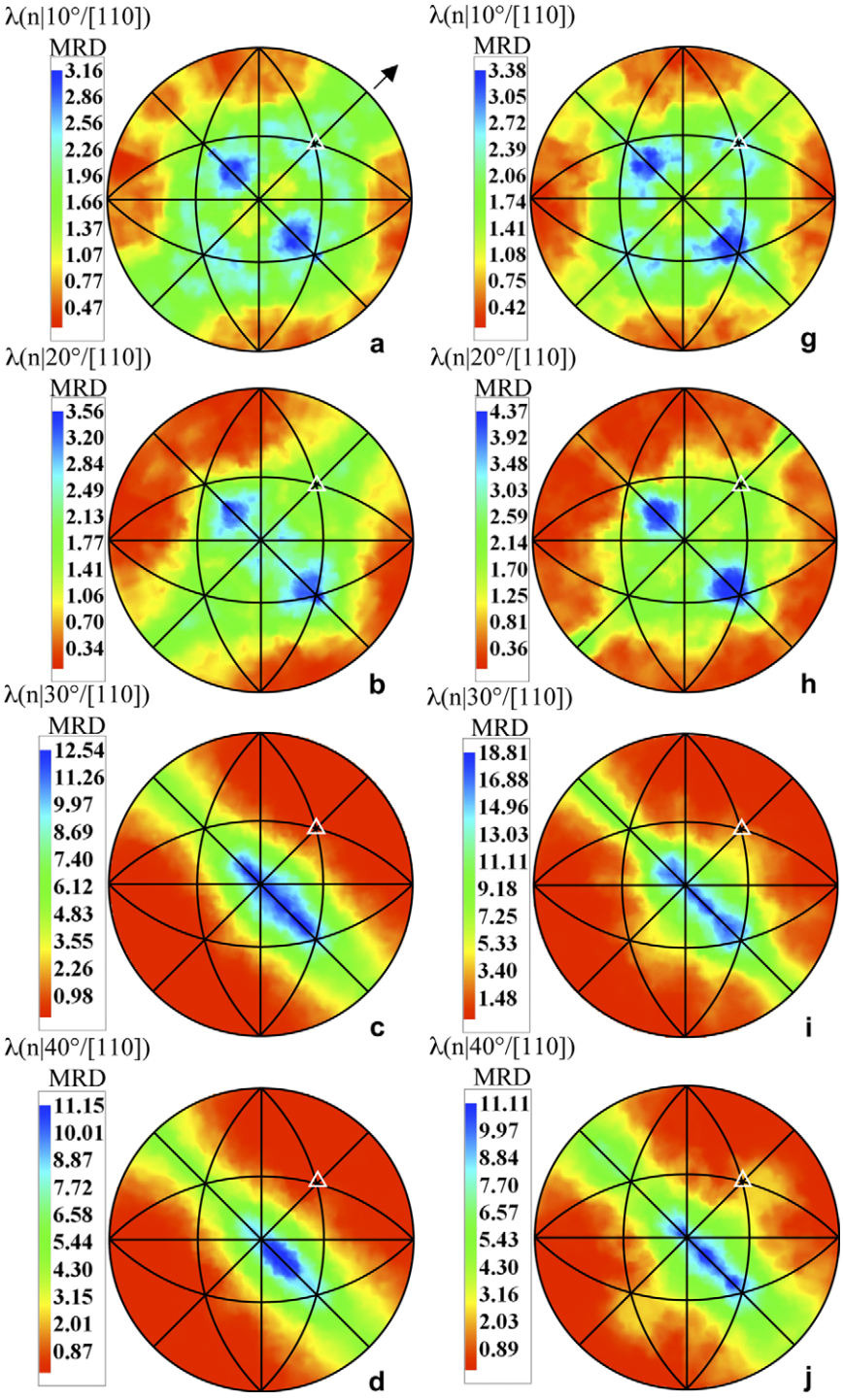

Fig. 4. Distribution of grain boundary planes for [1 1 0] misorientations, with Σ3 misorientations excluded. The misorientation angle increases in 10° increments. The data are plotted in stereographic projection along [0 0 1] and the reference frame is the same as in Fig. 3. The arrow in (a) shows the direction of the misorientation axis and the white triangle indicates the position of the [1 1 1] direction. Figures in the left-hand column (a–f) represent the reference sample and figures in the right-hand column (g–l) represent the ITMP sample.

this misorientation is symmetrically indistinguishable from the boundary obtained by a 146° rotation about the [7 7 1] axis and, because this direction is only 5.8° from [1 1 0], the zone of tilts is very near ⟨1 1 0⟩.

To estimate the fraction of Σ3 boundaries that was coherent, the observed grain boundary traces were compared to the traces that would be observed if the boundaries were coherent twins. Specifically, for every surface trace that was within Brandon's criterion of the ideal Σ3 misorientation, the angle it makes with the ideal coherent twin trace was calculated. These data are shown in Fig. 7. If the angle is less than the resolution of the

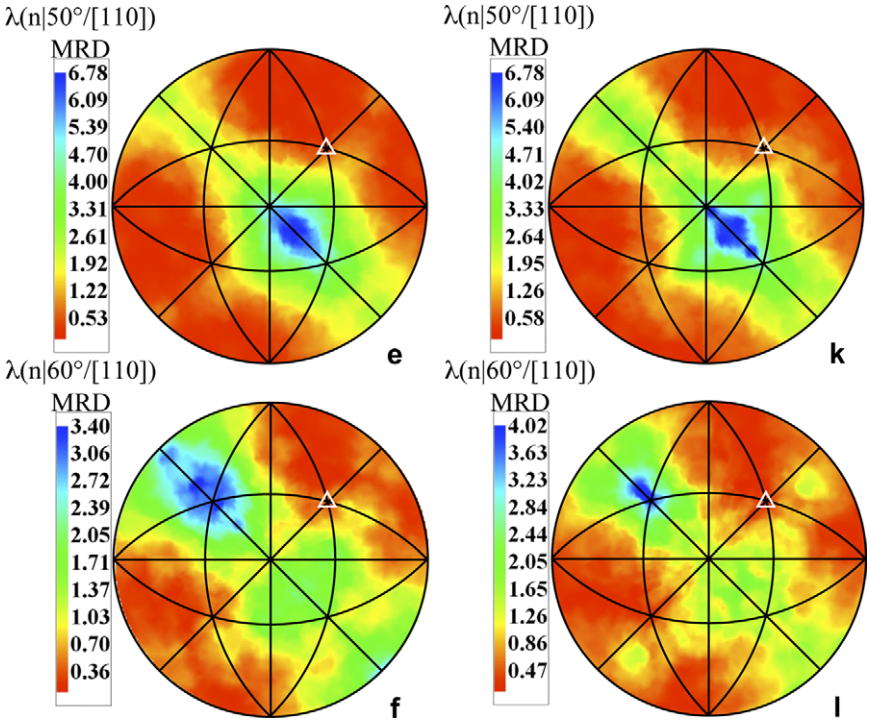

Fig. 4 (*continued*)

experiment (about 10°) it may be coherent. If the angle is greater, it is definitely not coherent. The majority of the traces have an orientation that is consistent with that expected for a coherent twin. It is noteworthy that essentially all of the additional Σ3 boundaries induced by the ITMP process are ideal, coherent twins. In other words, the added boundaries are annealing twins, which occur mostly within grains. These boundaries alter the grain boundary network only through the constraints they introduce at the positions where the twins join the network.

To understand how these twins influence the grain boundary network, we have analysed the distribution of triple junctions and how it is changed by the ITMP. In the reference sample, 52,000 triple junctions were analysed and, in the ITMP sample, 36,000 junctions were analysed. Boundaries were classified as Σ3, Σ9, Σ27, or *R*, where *R* is any other boundary, and the triple junctions were classified into four categories: J_0 junctions have three *R* boundaries, J_1 junctions have two *R* boundaries and a Σ3, Σ9, or Σ27 boundary, J_2 junctions have one *R* boundary and two twin-related boundaries (3,27, *R*; 9,27, *R*; 27,27, *R*; 9,9, *R*), and J_3 junctions have three twin related boundaries (3,3,9; 3,9,27; 9,9,9; 9,27,27). For J_1, J_2, and J_3 junctions, 3,*R*,*R*, 3,27,*R*, and 3,3,9, respectively, make up the most significant fraction of the total population. The fractions of each type of junction in both samples are illustrated in Fig. 8.

4. Discussion

The most striking aspects of the comparison between the reference and ITMP grain boundary character distributions are the similarities. As illustrated in Figs. 2–5, the basic features of the distributions are the same before and after the grain boundary engineering process. Two characteristic similarities, the tendency for boundaries to terminate on {1 1 1} planes and the high frequency of [1 1 0]-type tilt boundaries, are discussed first. The planes that occur with at least twice the relative area expected in the random distribution are either {1 1 1} (see Fig. 5) or {*hhk*}-type (see Fig. 4) in the [1 1 0] zone. The {1 1 1} planes are mostly twist boundaries that have a {1 1 1} plane on both sides of the boundary. It has been previously shown that the presence of two {1 1 1} planes at a grain boundary confers a lower than average energy, for all values of twist angle between the two {1 1 1} planes [6]. If the twist angle between the interfacing {1 1 1} planes is 60°, then the boundary is a coherent twin, which represents an energy minimum.

When the Σ3 CSL boundaries are included in the data set, the relative areas for the coherent twins, $\lambda([1\,1\,1]|60°/[1\,1\,1])$, are equal to 1500 MRD in the reference sample and 2200 MRD in the ITMP sample. When these boundaries are removed, there is still a peak at this position (see Fig. 5f and l), but the magnitude is reduced by more than two orders of magnitude. The boundaries that remain classified as Σ3 twins result from the fact that the criterion (Brandon's) used to partition the boundaries is not commensurate with the sizes of the discrete bins used to categorize the data. With this exception noted, the population of low-energy {1 1 1} twist boundaries is relatively independent of the twist angle. In particular, note that there is no enhancement of the population for the Σ7 misorientation, which is near 40°/[1 1 1]. Therefore, the high population of

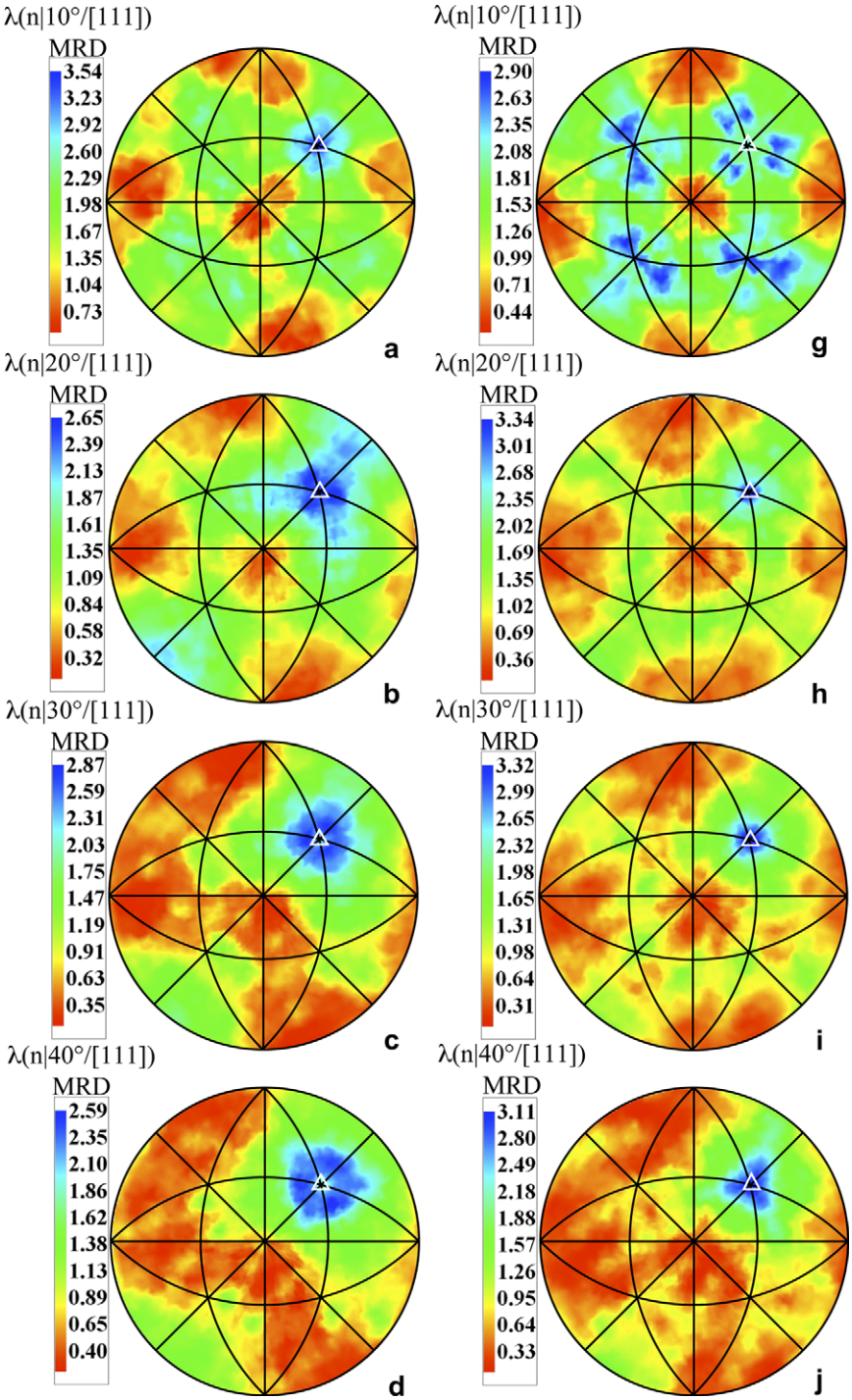

Fig. 5. Distribution of grain boundary planes for [1 1 1] misorientations, with Σ3 misorientations excluded. The misorientation angle increases in 10° increments. The data are plotted in stereographic projection along [0 0 1] and the reference frame is the same as in Fig. 3. The direction of the misorientation axis, [1 1 1] (which is inclined with respect to the plane of the page) is indicated by the white triangle. Figures in the left-hand column (a–f) represent the reference sample and figures in the right-hand column (g–l) represent the ITMP sample.

{1 1 1}-twist boundaries is not correlated to lattice coincidence, and is instead attributed to the presence of low-index, low-energy planes.

Following previous grain boundary population studies, we assume that grain boundaries with high populations in the distributions also have relatively low energies [6,12,22,23,32]. The energies of the boundaries are expected to be connected to their atomic structure and, in that light, it is of interest to compare the distribution of grain boundary planes in brass with those in Al, which also has fcc crystal structure [32]. Brass and Al are the only isostructural metals for which five-parameter data exist and can be compared. These two materials present and interesting contrast because of the difference in their stacking fault energy.

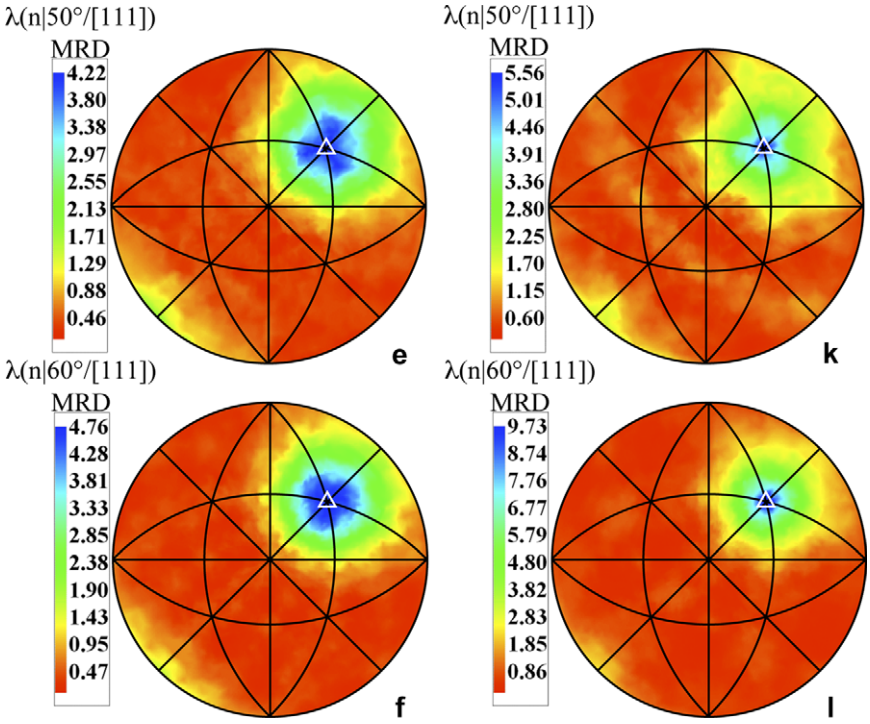

Fig. 5 (*continued*)

Because the density of annealing twins is inversely related to the stacking fault energy and Al has a relatively high stacking fault energy, annealing twins are observed infrequently [33,34]. Brass, in contrast, has a very low stacking fault energy and, as a result, annealing twins dominate the GBCD. Despite this large difference, when coherent twins are removed from the data set, the distribution of grain boundary planes, $\lambda(\mathbf{n})$, irrespective of misorientation, is nearly indistinguishable in brass and Al. This observation suggests that because {1 1 1} is the closest packed, lowest energy plane in fcc crystals, the preference is a general feature of all materials with this structure.

Grain boundary planes separating crystals with [1 1 0] misorientations have orientations that are spread along the [1 1 0] zone, indicating that they are predominantly asymmetric tilt grain boundaries. This situation is quite different from the findings in Al, where the [1 1 0] tilt boundaries were generally symmetric [32]. Furthermore, grain boundaries with [1 1 0] type misorientations occur more frequently in brass than in Al. Excluding the effects of Σ9 and Σ27, the peak values in the grain boundary plane distributions for [1 1 0] boundaries in brass are in the range 3–6 MRD. In Al, the same distributions peaked between 2 and 3 MRD [32]. The higher frequency of tilt boundaries in brass may result from the constraints imposed by the presence of coherent twins. In the reference sample, 63.0% of all triple junctions contain at least one Σ3 grain boundary and the vast majority are coherent twins. In the ITMP sample, the fraction of triple junctions containing at least one Σ3 grain boundary is 76.1%. So, when a grain boundary with a [1 1 0] type misorientation intersects other boundaries at a triple junction, it is more likely to meet a coherent twin than any other type of boundary. There are two features of this geometry that influence the distribution. First, the twinned grains (see 1 and 2 in Fig. 9) share a common ⟨1 1 0⟩ axis (in the twin boundary) so that if the third crystal is misoriented about a ⟨1 1 0⟩ axis with respect to the first crystal, then it is also misoriented about a ⟨1 1 0⟩ axis with respect to the second crystal. In other words, if a twin and a boundary with a ⟨1 1 0⟩ misorientation meet at a triple junction, the third boundary must also have a ⟨1 1 0⟩ misorientation (although its disorientation might be along another axis), as illustrated schematically in Fig. 9. This effect tends to increase the number of ⟨1 1 0⟩ type boundaries in proportion to the number of twins. The second important feature of this geometry is that the boundary plane of the twin is fixed and this constrains the triple line direction. Thus, the coherent twin removes one degree of freedom from the triple line's orientation. If any of the other grain surfaces have a ⟨1 1 1⟩ orientation, then the direction of the triple line is fixed at the intersection of these two planes, which must be a ⟨1 1 0⟩ direction. This direction is also the common axis between the grains. In this case, the two grain boundaries in the triple junction are therefore confined to the [1 1 0] zone and the boundaries are guaranteed to be tilt boundaries. So, the high relative areas of [1 1 0] type boundaries can be explained by the fact that when one such boundary meets a coherent twin, another [1 1 0] type is generated. The fact that most of these boundaries are tilt boundaries can be explained by the relatively high incidence of {1 1 1} grain boundary planes which, when coupled with a coherent

twin, forces the triple line direction to have ⟨1 1 0⟩ character.

Previous work has highlighted reasons for the prevalence of asymmetric boundaries, as opposed to symmetric types, in polycrystals [35,36]. From a probability point of view, there are many more possible asymmetric boundaries than symmetric ones, even when only tilt boundaries and low-index planes are considered. Geometrical constraints dictate that an asymmetrical boundary usually comprises only one low-index plane, because once the indices of the plane on one side of the boundary are selected, the indices of the second plane are fixed by the misorientation. There is no evidence of a strong preference for symmetrical planes in the current data. Whereas the MRD values at the locations of the symmetrical planes are relatively high, they are not greater than the populations of the asymmetric planes in the same zone. As mentioned in Section 1, a preference for asymmetrical tilt boundaries has been noted previously both from HREM observations [35] and from other measurements of boundary planes [20,21,23].

The differences between the GBCD before and after the ITMP treatment can be summarized as follows:

- The number fraction and relative area of boundaries with the Σ3, Σ9, and Σ27 misorientations increase. The added grain boundary planes do not have the same distribution as the pre-existing population.
- The Σ3 grain boundaries added to the microstructure are nearly all coherent twins.
- The number of boundaries terminated by {1 1 1} planes increases, even when coherent twins are removed from the population.
- The number of ⟨1 1 1⟩ twist boundaries increases.
- The number of triple junctions between three random boundaries decreases and the number of triple junctions with three $\Sigma 3^n$ boundaries increases.

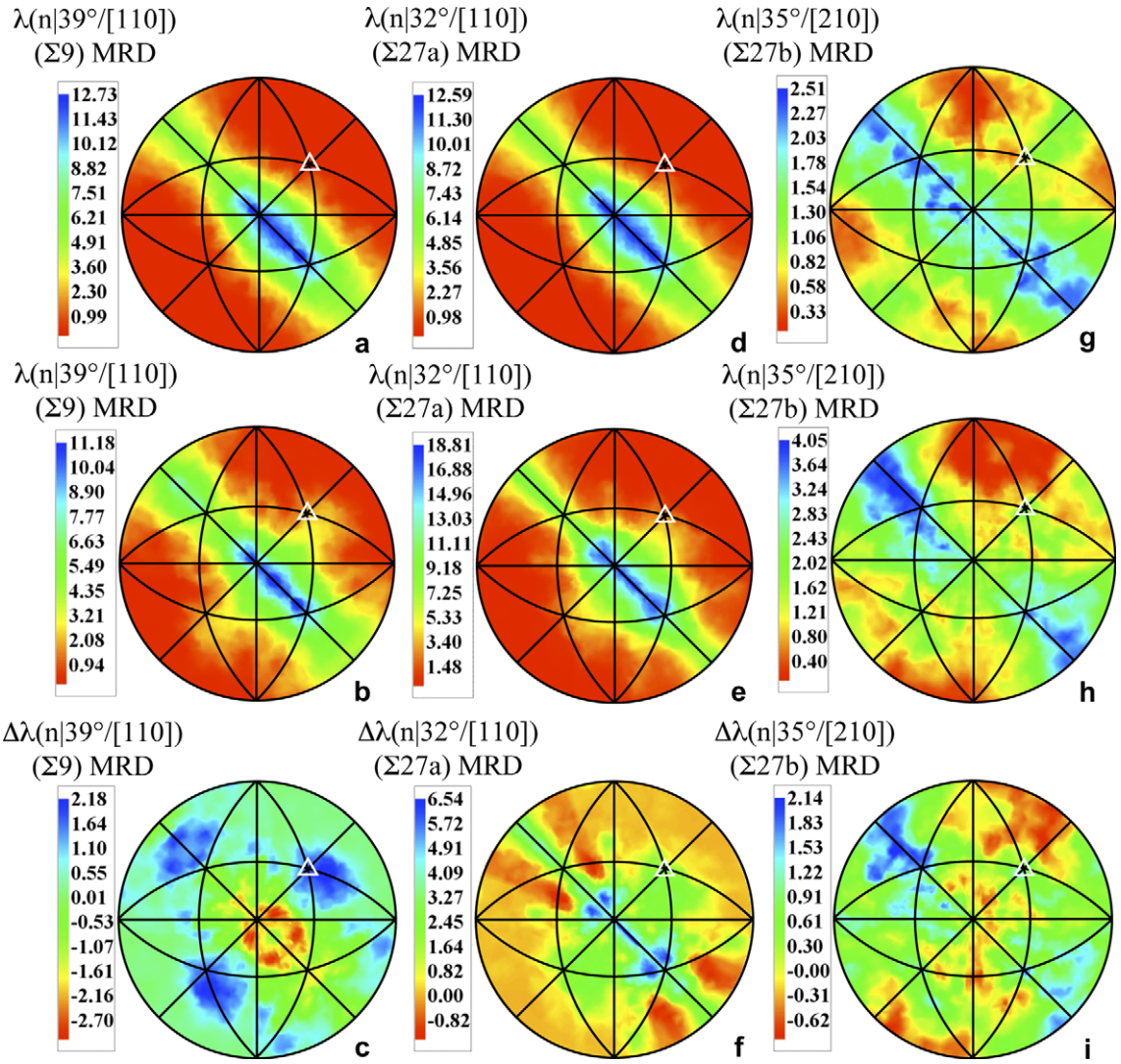

Fig. 6. Distribution of grain boundary planes for Σ9, Σ27a, and Σ27b misorientations. The distributions for the reference sample are shown in (a), (d), and (g) (top row). The distributions for the ITMP sample are shown in (b), (e), and (h) (middle row). The distributions in (c), (f), and (i) (bottom row) are the differences between (a) and (b), (d) and (e), and (g) and (h), respectively.

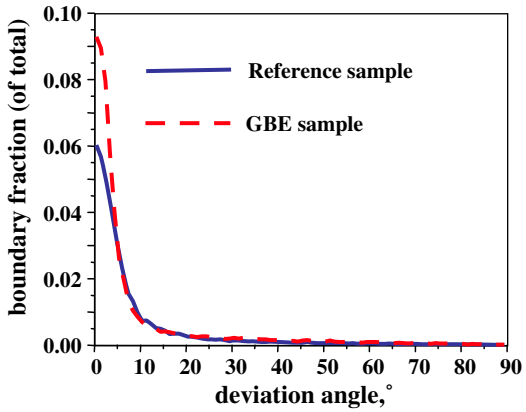

Fig. 7. The distribution of deviation angles between the observed Σ3 grain boundary traces and the ideal traces expected for coherent twin boundaries, for the reference and ITMP samples.

These data have significant implications regarding the mechanisms of the ITMP. The most obvious difference is the increase in Σ3s after ITMP, which is the fundamental feature of all ITMP investigations. The majority of Σ3 length is annealing twins, which are not part of the 'grain boundary network'. The consequence of twinning on ITMP is therefore how it constrains other interfaces in the grain boundary network when they are joined by a twin. One such constraint is that the combination of two Σ3 boundaries always creates a $\Sigma 3^n$, forming a J_3-type junction. As the concentration of Σ3 boundaries increases, they are more likely to intersect one another, and when this happens a Σ9 boundary must be formed [37]. Thus, the number of Σ9 boundaries is expected to increase in proportion to the number of Σ3 boundaries. Similarly, when a Σ3 boundary meets a Σ9, it produces either another Σ3 or a Σ27. The effect of Σ3 impingement on systematic increases in the concentration of Σ9 and Σ27 grain boundaries in metals with a high density of annealing twins has been reported by others [38]. The data in Fig. 7 show a clear increase in the number of J_3-type junctions comprised of three $\Sigma 3^n$ boundaries and we therefore conclude that the increased concentration of Σ9 and Σ27 boundaries is a consequence of the increase in the concentration of Σ3 boundaries.

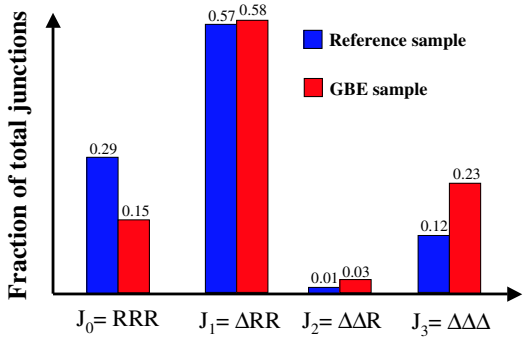

Fig. 8. Number fraction of different types of triple junctions in the reference and ITMP samples, where Σ refers to Σ3, Σ9, and Σ27.

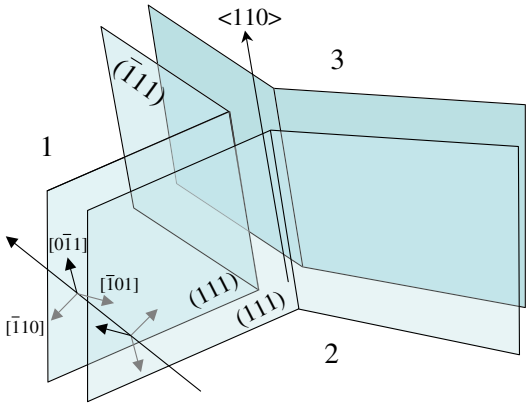

Fig. 9. Schematic illustration of a triple junction with one of the boundaries (between crystals 1 and 2) constrained to be a coherent twin. The bounding planes of each boundary are shown separated, to emphasize their association with the adjoining crystals. The coherent twin condition constrains a common [1 1 1] axis to be perpendicular to the boundary and a common ⟨1 1 0⟩ axis to be parallel to the boundary. If one more plane has a {1 1 1}, as illustrated here, then the triple line is fixed in a ⟨1 1 0⟩ direction.

The orientations of the Σ27 grain boundaries that were added by the ITMP are comparable to those existing in the reference sample. For both the Σ27a (see Fig. 6f) and Σ27b boundaries (see Fig. 6i), the orientations of the new boundaries are mostly near {*hhk*} types. For the Σ27a, this is anticipated from the constraint at triple junctions with a common [1 1 0] direction that contain a coherent twin and another grain boundary plane in the {1 1 1} orientation, as discussed above.

The orientations of the Σ9 grain boundaries that were added by the ITMP are distinct from those already in the reference sample (see Fig. 6c). One peak is in the vicinity of one of the symmetric tilt grain boundaries with the $[\bar{2}21]$ orientation. The other two peaks are at positions corresponding to mixed boundaries, with orientations near (1 1 1) and $(\bar{1}\bar{1}1)$. These mixed boundaries are a minority fraction of all Σ9 boundaries and are outnumbered by the tilt boundaries on the [1 1 0] zone. However, given the arguments for the generation of tilt boundaries at other misorientations, this observation is puzzling. The most significant change in the number of Σ9 boundaries can be correlated to the increase in the number of J_3 junctions (see Fig. 8). The number of J_3 junctions of the type 3, 3, 9, increased by 70% (from 10% to 17% after ITMP). In the cases where the Σ3 boundaries are coherent twins, the boundary plane of the Σ9 plane must be a tilt boundary and this explains the $[\bar{2}21]$ peak. If one of the Σ3 boundaries is not a twin, the Σ9 boundary plane is not constrained, and this situation can contribute to the peaks near (1 1 1) and $(\bar{1}\bar{1}1)$ in Fig. 6c. Because the new Σ9 segments frequently form short connections between two Σ3 boundaries, they have less freedom with respect to their orientation and the triple line might be less likely to form with a [1 1 0] orientation. These cases might explain the mixed tilt-twist boundaries in Fig. 6c. The number of J_3 junctions of the type 3,9,27 tripled

(from 2% to 6%). In this case, the boundary will be a tilt type only if the Σ3 is a twin and another plane is {1 1 1}, as discussed above.

Although the numbers of Σ9 and Σ27 boundaries are relatively small in comparison to the Σ3 boundaries, they are significant because they arise as a geometrical consequence of Σ3 interactions. The question arises as to whether Σ9s and Σ27s are truly 'special' in the sense that they have markedly better than average properties. We have not evaluated the properties of individual boundaries, but following the prior work described in Section 1, it is assumed that low grain boundary energies and high populations are strong indicators of special properties. Therefore, if the Σ9 and Σ27 boundaries are asymmetric tilt boundaries with low index planes, they are special. The spread in the boundary planes along the [1 1 0] zone in Fig. 4 is consistent with this condition and we conclude that they are special. Conversely, the minority boundaries with the Σ9 and Σ27 misorientation but general planes, are not special. Other tilt boundaries on ⟨1 1 0⟩, which have a relatively high population, can also be special, depending on the planes that constitute the boundary.

The implication of this work for ITMP is that an increased proportion of annealing twins has resulted in modifying the grain boundary network to include an increased proportion of both {1 1 1} planes and asymmetric tilt grain boundaries misoriented on ⟨1 1 0⟩. We conclude that these boundaries are 'special', and that ITMP is based on selection of special planes rather than misorientations. Finally, these insights could not have been gained without the five-parameter analysis.

5. Conclusions

The five-parameter GBCD has been determined in brass before and after ITMP. The main findings were:

1. In both the reference and ITMP specimens there was a tendency for boundaries to terminate on low-index planes. These planes were either {1 1 1}, many of them twist boundaries, or planes on the ⟨1 1 0⟩ zone which have arisen as ⟨1 1 0⟩ tilt boundaries. Most of the ⟨1 1 0⟩ tilt boundaries are asymmetric. The increased population of low-index plane boundaries is associated with their low energy.
2. The main differences between the reference and the ITMP specimens were that after ITMP there was an increase in the relative areas of the grain boundaries with the Σ3, Σ9, and Σ27 misorientation. The Σ3 boundaries that arose during ITMP were overwhelmingly coherent twins. There was also an increase in proportion of {1 1 1} planes (even when Σ3s were excluded), there were more ⟨1 1 0⟩ asymmetric tilts, and there were more ⟨1 1 1⟩ twist boundaries. These increases correspond to an increase in the proportion of low-index planes at boundaries.
3. The number of triple junctions between three random boundaries decreased. The fraction of grain boundary triple junctions formed between Σ3, Σ3, and Σ9 boundaries increased by 70% after ITMP and the fraction of triple junctions formed between Σ3, Σ9, and Σ27 boundaries increased by a factor of three.
4. The five-parameter data recorded in this investigation add strength to the previously made suggestion that 'special' boundaries are those that terminate on low-index planes.
5. It is suggested that the high relative areas of ⟨1 1 0⟩ type boundaries can be explained by the fact that when one such boundary meets a coherent twin, another such boundary is generated. The fact that most of these boundaries have the tilt configuration can be explained by the relatively high incidence of {1 1 1} grain boundary planes, which when coupled with a coherent twin, forces the triple line direction to have ⟨1 1 0⟩ character.
6. Σ9 and Σ27 boundaries are geometrically necessary where there is multiple twinning. Whether or not they are 'special' depends on if they have low-index planes.
7. The broad features of the GBCDs recorded here are expected to be general for all fcc metals which twin readily.

Acknowledgements

The work at Carnegie Mellon University was supported primarily by the MRSEC program of the National Science Foundation under Award Number DMR-0520425. The work at Swansea was partially supported by the Engineering and Physical Sciences Research Council.

References

[1] Kumar M, Schuh CA, editors. Viewpoint set no. 40, Scripta Mater 2006;54:961.
[2] Lin P, Palumbo G, Erb U, Aust KT. Scripta Metall Mater 1995;33:1387.
[3] Randle V. Acta Mater 2004;52:4067.
[4] Randle V. Mater Charact 2001;47:411.
[5] Merkle KL. J Phys Chem Solids 1994;55:991.
[6] Merkle KL, Wolf D. Philos Mag 1992;65A:513.
[7] Hasson GC, Goux C. Scripta Metall 1971;5:889.
[8] Dhalenne G, Dechamps M, Revcolevschi A. J Am Ceram Soc 1982;65:C11.
[9] Kimura S, Yasuda E, Sakaki M. Yogyo-Kyokai-Shi 1986;94:795.
[10] Schmelzle R, Muschik T, Gust W, Predel B. Scripta Metall Mater 1991;25:1981.
[11] Wolf U, Ernst F, Muschik T, Finnis MW, Fischmeister HF. Philos Mag A 1992;66:991.
[12] Saylor DM, Morawiec A, Rohrer GS. Acta Mater 2003;51:3675.
[13] Amouyal Y, Rabkin E, Mishin Y. Acta Mater 2005;53:3795.
[14] Miyamoto H, Ikeuchi K, Mimaki T. Scripta Mater 2004;50:1417.
[15] Lejcek P, Paidar V. Scripta Metall Mater 1994;30:283.
[16] Krakauer BW, Seidman DN. Acta Mater 1998;46:6145.
[17] Lejcek P, Paidar V. Mater Sci Technol 2005;21:393.
[18] Wynblatt P, Takashima M. Interf Sci 2001;9:265.
[19] Saylor DM, El-Dasher BS, Pang Y, Miller HM, Wynblatt P, Rollett AD, et al. J Am Ceram Soc 2004;87:724.

[20] Rohrer GS, Saylor DM, El-Dasher BS, Adams BL, Rollett AD, Wynblatt P. Z Metallkd 2004;95:197.
[21] Saylor DM, Morawiec A, Rohrer GS. Acta Mater 2003;51:3663.
[22] Saylor DM, Morawiec A, Rohrer GS. J Am Ceram Soc 2002;85:3081.
[23] Saylor DM, El-Dasher BS, Sano T, Rohrer GS. J Am Ceram Soc 2004;87:670.
[24] Gruber J, George DC, Kuprat AP, Rohrer AD, Rollett GS. Scripta Mater 2005;53:351.
[25] Kim C, Hu Y, Rohrer G, Randle V. Scripta Mater 2005;52:633.
[26] Randle V, Davies H. Mater Trans 2002;33A:1853.
[27] Clark WAT, Wagoner RH, Shen ZY, Lee TC, Robertson IM, Birnbaum HK. Scripta Metall Mater 1992;26:203.
[28] Saylor DM, Adams BL, El-Dasher BS, Rohrer GS. Metall Mater Trans 2004;35A:1981.
[29] Wright SI, Larsen RJ. J Microsc 2002;205:245.
[30] Randle V. Interf Sci 2002;10:271.
[31] Kogtenkova O, Straumal B, Protosova S, Tsurekawa S, Watanabe T. Z Metallkd 2005;96:216.
[32] Saylor DM, El-Dasher BS, Rollett AD, Rohrer GS. Acta Mater 2004;52:3649.
[33] Gleiter H. Acta Metall 1969;17:1421.
[34] Christian JW, Swann PR. Alloying behavior and effects in concentrated solid solutions. New York (NY): Gordon and Breach Science; 1965. p. 105.
[35] Merkle KL. Scripta Metall 1989;23:1487.
[36] Merkle KL. Ultramicroscopy 1991;37:130.
[37] Miyazawa K, Iwasaki Y, Ito K, Ishida Y. Acta Crystallogr 1996;A52:787.
[38] Lim LC, Raj R. Acta Metall 1984;32:1177.